Materials
Advances

rsc.li/materials-advances

**ROYAL SOCIETY
OF CHEMISTRY**
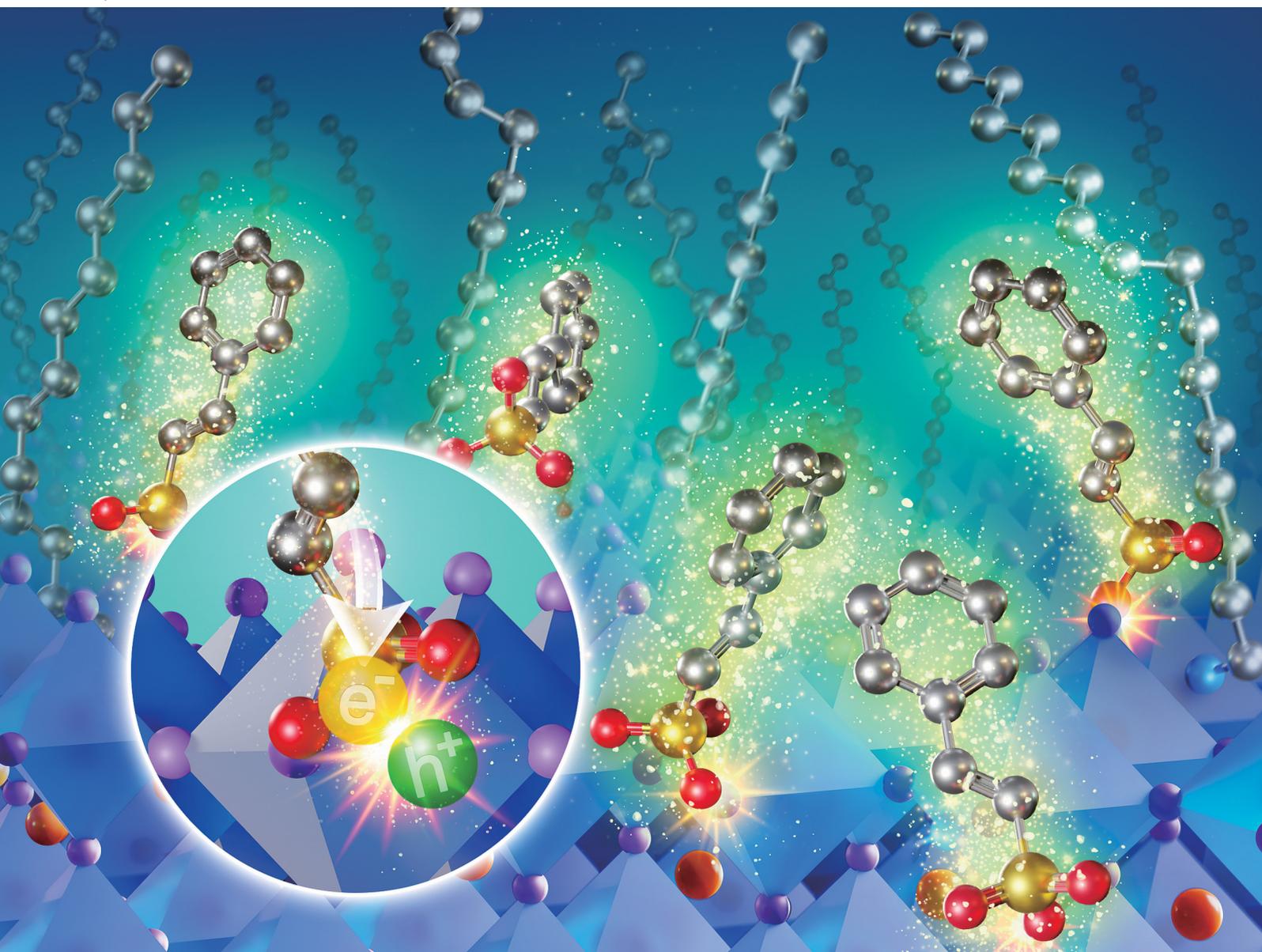
PAPER
Chen-Hsuan Kuan and Sheng-Hsiung Yang
Surface ligand engineering of perovskite nanocrystals with a
conjugated sulfonate ligand for light-emitting applications

PAPER

Check for updates

Surface ligand engineering of perovskite nanocrystals with a conjugated sulfonate ligand for light-emitting applications†

Chen-Hsuan Kuan and Sheng-Hsiung Yang 🆔 *

All-inorganic perovskite ($CsPbX_3$, X = Cl, Br, or I) nanocrystals (NCs) with superior optical and optoelectronic properties are regarded as potential active materials for light-emitting applications. However, the commonly used insulating ligands such as oleylamine (OAm) and oleic acid (OA) with long hydrocarbon chains on the surface of perovskite NCs lead to low device performance of perovskite light-emitting diodes (PeLEDs). In this study, we introduced a new sulfonate ligand sodium beta-styrenesulfonate (SβSS) with elongated π-conjugation in the surface ligand engineering of $CsPbBr_3$ NCs. The results show that the sulfonate ligand was successfully anchored on the surface of $CsPbBr_3$ NCs, which can decrease the surface defects and improve the photoluminescence quantum yield (PLQY) from 53 to 75% compared with the pristine perovskite NCs. Moreover, its π-conjugation can also enhance the charge injection and transport capability. The optimized green PeLED based on the SβSS-modified $CsPbBr_3$ NCs exhibited a maximum brightness of 10 965 cd m^{-2} and a maximum current efficiency of 10.9 cd A^{-1}, revealing 2.5- and 2.4-fold enhancement compared with the device based on pristine NCs.

1. Introduction

All-inorganic cesium lead halide ($CsPbX_3$, X = Cl, Br, and I) perovskite nanocrystals (NCs) have drawn a great deal of attention owing to several promising advantages, such as low cost, solution processability, a tunable bandgap (E_g), narrow full width at half-maximum (FWHM), and high photoluminescence quantum yield (PLQY).[1–3] The above perovskite NCs have been utilized in the fields of light-emitting diodes,[4–6] solar cells,[7–9] lasers,[10,11] scintillators,[12] and photodetectors.[13,14] To date, several synthetic methods have been proposed to synthesize perovskite NCs, including the hot injection,[15–18] ligand-assisted re-precipitation,[19–22] solvothermal synthesis,[23] ultrasonication,[24] and microwave-assisted synthesis.[25] The hot injection method remains the most popular approach to prepare perovskite NCs with uniform crystalline size, excellent luminescence properties, and superior stability.

It is well known that carrier injection from charge transport layers into perovskite emitters is essential to form charge recombination for perovskite light-emitting diodes (PeLEDs).

Two major issues are generally considered for the development of high-quality perovskite emitters. First, highly dynamic binding between the perovskite surface and long-chain capping ligands such as oleylamine (OAm) and oleic acid (OA) usually results in the chemical instability of perovskite NCs.[26] Second, those OAm and OA ligands containing long insulating hydrocarbon chains hinder charge injection and transport, therefore charge recombination within perovskite NCs is reduced.[27] To overcome the problems, several techniques have been proposed. Zeng *et al.* demonstrated solution purification of perovskite NCs by using a hexane/ethyl acetate mixed solvent to fine-tune the surface ligand density,[28] achieving surface passivation and carrier injection by removing excess ligands with long alkyl chains. As a result, 50-fold external quantum efficiency (EQE) improvement of PeLEDs was achieved. Apart from solution purification, the incorporation of novel functional ligands is also adopted to improve charge transport capability and further enhance device performance. Several quaternary ammonium bromide ligands, such as didodecyldimethylammonium bromide and didecyldimethyl ammonium bromide,[29–31] were utilized to partially replace OAm and OA ligands. The charge transport capability as well as stability of capped perovskite NCs was significantly improved and thus the corresponding PeLED performance was enhanced. Some short chain ligands carrying acid groups other than the carboxylate group, including octylphosphonic acid and sodium dodecyl sulfate,[32–34] have also been

Institute of Lighting and Energy Photonics, College of Photonics, National Yang Ming Chiao Tung University, No. 301, Section 2, Gaofa 3rd Road, Guiren District, Tainan, 71150, Taiwan, Republic of China. E-mail: yangsh@nycu.edu.tw

introduced onto the perovskite surface. Due to the strong interaction between those ionic ligands and Pb atoms, reduced surface defects, enhanced stability and efficient charge injection were obtained. The third type of surface ligand with π-conjugation, for instance, 3-phenyl-2-propen-1-amine, 2,2′-iminodibenzoic acid, phenethylammonium bromide, phenethylammonium iodide, and diphenylammonium bromide,[35–39] was proposed by different research groups to passivate surface trap states of perovskite NCs. A remarkable enhancement in stability and carrier transport was achieved by replacing the long insulating ligands with π-conjugated ones. Besides the abovementioned types of ligands, 1,3-adamantanedicarboxylic acid, 1,8-octyldiamine bromide salt, and tris(2-aminoethyl)ammonium bromide have also been introduced onto the surface of perovskite NCs to reduce surface defects for enhancing the performance of perovskite NCs.[40–42]

Based on the above consideration, we utilize a conjugated sulfonate ligand, namely sodium beta-styrenesulfonate (SβSS), to anchor on the surface of CsPbBr$_3$ NCs in the surface ligand engineering of CsPbBr$_3$ NCs for passivation. The chemical structure of SβSS is shown in Fig. 1a. The features of this ligand include elongated π-conjugation and strong binding with Pb atoms through the sulfonate group, which are beneficial for high-quality perovskite NCs with enhanced conductivity. To the best of our knowledge, this sulfonate ligand has not been investigated for perovskite NCs so far. The schematic illustration of the synthesized CsPbBr$_3$ NCs capped with SβSS ligands is depicted in Fig. 1b, revealing a longer PL lifetime and a higher PLQY compared with pristine CsPbBr$_3$ NCs without the SβSS ligand. Fig. 1c demonstrates the surface passivation mechanism of SβSS on CsPbBr$_3$ NCs. The pristine NCs have many uncoordinated Br$^-$ vacancies on the perovskite surface, which usually cause severe nonradiative recombination and lower device performance. The SβSS ligand can occupy those Br$^-$ vacancies and therefore passivate the surface defect. PeLEDs based on the SβSS-modified CsPbBr$_3$ NCs were further fabricated and evaluated, exhibiting a maximum brightness (L_{max}) of 10 965 cd m^{-2} and a maximum current efficiency (η_{max}) of 10.9 cd A^{-1}. Our results demonstrate that SβSS is capable of being an effective ligand in the synthesis of perovskite NCs for surface passivation and carrier injection.

2. Experimental section

2.1 Materials

Indium tin oxide (ITO) glass substrates (15 Ω sq^{-1}) were purchased from Aimcore Technology. Cesium carbonate (Cs$_2$CO$_3$, purity 99.99%), OAm (purity 80–90%), 1-octadecene (ODE, purity 90%)

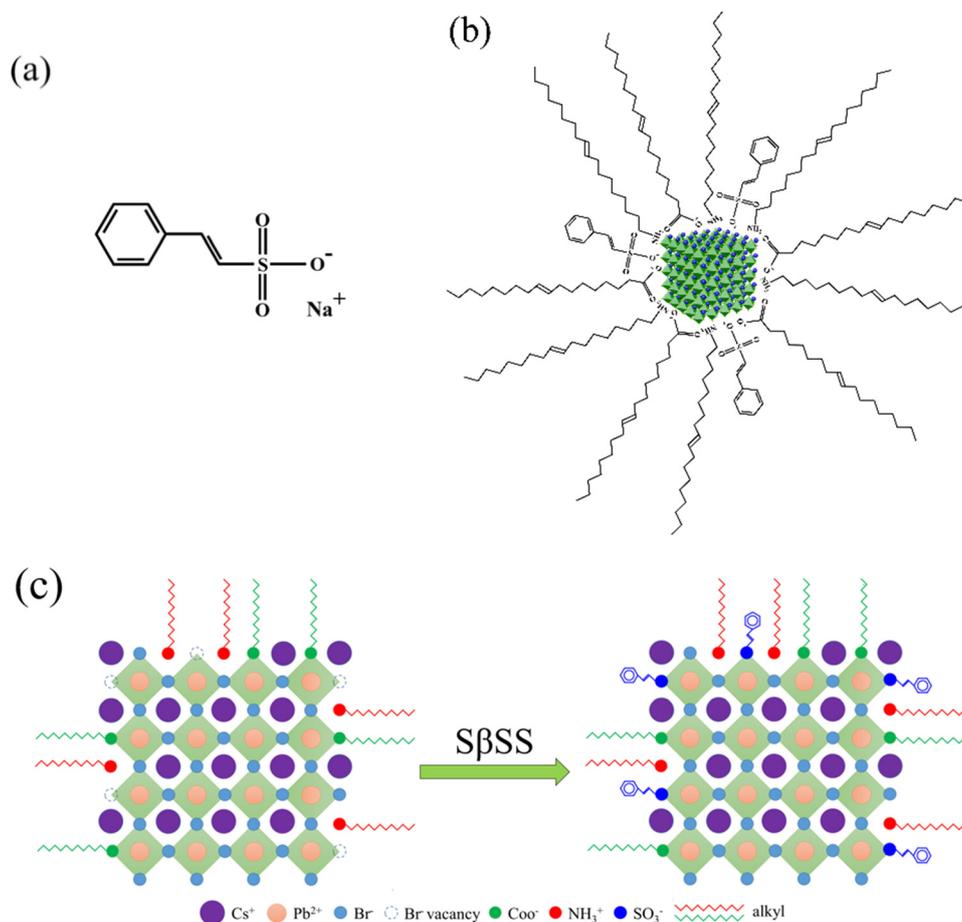Fig. 1 (a) Molecular structure of SβSS, (b) schematic illustration of the SβSS-modified CsPbBr$_3$ NCs, and (c) surface passivation mechanism on CsPbBr$_3$ NCs.

were purchased from Acros. OA (purity 90%) and poly(4-butyl-phenyl-diphenylamine) (Poly-TPD) were purchased from Sigma-Aldrich. Lead(II) bromide ($PbBr_2$, purity 99.998%) and SβSS (purity > 95.0%) were purchased from Alfa Aesar and TCI, respectively. Poly(3,4-ethylenedioxythiophene):polystyrene sulfonate (PEDOT:PSS) aqueous solution (Clevios PVP AI 4083) was purchased from Heraeus Precious Metals GmbH & Co. KG. 1,3,5-Tris(1-phenyl-1H-benzimidazol-2-yl)benzene (TPBi) was purchased from Shine Material Technology. Other organic solvents were bought from DUKSAN, MACRON, and TEDIA and used without further purification.

2.2 Synthesis of the Cs-oleate

The Cs-oleate was prepared according to the previous literature and some modifications were made in this study.[31] Cs_2CO_3 (0.407 g, 1.25 mmol), OA (1.25 mL), and ODE (20 mL) were loaded into a 50 mL two-neck flask and degassed under vacuum at 120 °C for 1 h. Afterward, the mixture was heated to 160 °C under a nitrogen atmosphere until all solid was dissolved.

2.3 Synthesis of the pristine and SβSS-modified $CsPbBr_3$ NCs

$PbBr_2$ (0.069 g, 0.188 mmol), OA (0.3 mL), OAm (0.5 mL), and ODE (5 mL) were loaded into a 50 mL two-neck flask and degassed under vacuum at 120 °C for 1 h, followed by nitrogen purge for 20 min. Afterward, the mixed solution was heated to 160 °C and 0.4 mL of Cs-oleate was quickly injected. After 5 s, the flask was immersed in an ice bath to obtain pristine $CsPbBr_3$ NCs. To synthesize the SβSS-modified $CsPbBr_3$ NCs, 5 (0.024 mmol), 10 (0.047 mmol), or 20 mg (0.097 mmol) of SβSS were added to the abovementioned $PbBr_2$ solution. The synthetic procedure was the same as that of pristine $CsPbBr_3$ NCs.

2.4 Purification of pristine and SβSS-modified $CsPbBr_3$ NCs

The crude solution was centrifuged at 8500 rpm for 5 min. The precipitate was collected and dispersed in 2 mL of n-hexane. Afterward, 8 mL of ethyl acetate was added and the mixture was centrifuged again at 8500 rpm for 5 min. Finally, the purified precipitate was dispersed in n-hexane for materials characterization and device fabrication.

2.5 Device fabrication

The light-emitting devices with a regular configuration of ITO/PEDOT:PSS/Poly-TPD/pristine or SβSS-modified $CsPbBr_3$ NCs/TPBi/LiF/Al were fabricated. The ITO substrate was cleaned sequentially with detergent, deionized water, acetone, and isopropanol under ultrasonication for 20 min, followed by nitrogen purging and ultraviolet-ozone treatment for 25 min. The PEDOT:PSS solution (filtered through a 0.22 μm nylon filter) was spin-cast onto the cleaned ITO substrate at 3000 rpm for 30 s and baked at 150 °C for 15 min in air. The substrate was then transferred into a nitrogen-filled glovebox. Poly-TPD (in chlorobenzene, 6 mg mL^{-1}) was deposited on top of PED-OT:PSS by spin-coating at 3000 rpm for 30 s, followed by drying at 150 °C for 20 min. The $CsPbBr_3$ NC dispersion after filtration by PTFE syringe filters was spin-coated onto the Poly-TPD layer and baked at 70 °C for 10 min. Finally, 35 nm of TPBi, 1 nm of

LiF, and 100 nm of aluminum electrodes were deposited sequentially by thermal evaporation under a base pressure of $\sim 10^{-6}$ Torr. The active area of each device is 1 mm^2.

2.6 Characterization methods

The morphology and size of $CsPbBr_3$ NCs were examined with a JEOL JEM-1400 transmission electron microscope (TEM). The high-resolution (HR) TEM images of individual $CsPbBr_3$ NCs were obtained from a JEOL 3010 TEM. The elemental mapping of all $CsPbBr_3$ NCs without and with the SβSS ligand was performed on a FEI E.O Tecnai G2 F20 TEM. The cross-sectional micrographs of samples were investigated with an ultrahigh resolution ZEISS Crossbeam scanning electron microscope (SEM). The Fourier transform infrared (FT-IR) spectra were measured using a Thermo Scientific Nicolet iS-10 spectrometer. Nuclear magnetic resonance (NMR) spectra were recorded on a Bruker AV-500 NMR spectrometer. The absorption, photoluminescence (PL), and PLQY of samples were recorded with a Princeton Instruments Acton 2150 spectrophotometer equipped with a xenon lamp as the light source. To perform time-resolved PL (TR-PL) measurements, a 473 nm pulsed laser (Omicron) was utilized as an excitation light source. The TR-PL signals were recorded by a time-correlated single-photon counting module (PicoQuant MultiHarp 150 4N) combined with a photomultiplier tube through an Andor Kymera 328i spectrometer. The apparatus was assembled by LiveStrong Optoelectronics Co., Ltd., Taiwan. The X-ray diffraction (XRD) patterns of samples were measured with a Bruker D8 Discover diffractometer. X-Ray photoelectron spectroscopy (XPS) measurements were conducted using a Thermo K-Alpha XPS instrument for elemental composition analysis of $CsPbBr_3$ NCs without or with SβSS. The performance and electroluminescent (EL) spectra of light-emitting devices were recorded using an Agilent 4155C semiconductor parameter analyzer and an Ocean Optics USB2000+ spectrometer.

3. Results and discussion

The SβSS ligand was introduced onto the surface of $CsPbBr_3$ NCs at different amounts of 5, 10, and 20 mg in this study. The pristine $CsPbBr_3$ was also synthesized for comparison. Fig. 2(a–d) show different $CsPbBr_3$ NCs with various SβSS contents, revealing similar cubic crystalline form and size. The size distribution of NCs is displayed Fig. S1 in the ESI.† It is seen that the average crystallite size decreased from 12.1 to 11.43 nm with increasing SβSS amount, which can be explained by the fact that the surface ligand limits the growth of $CsPbBr_3$ NCs.[34] The insets in Fig. 2(a–d) show a lattice spacing of 0.58 nm, which corresponds to the (100) plane of the cubic perovskite structure.[43–46] The XRD patterns of $CsPbBr_3$ NCs without and with the SβSS ligand are shown in Fig. 2e. All samples possess four significant diffraction peaks at 2θ = 15.1, 21.4, 30.4, and 37.5°, indicative of the (100), (110), (200), and (211) planes, respectively, which match well with the cubic phase.[46] No additional diffraction peaks were found and we speculate that the crystalline structure of $CsPbBr_3$ NCs is independent of the dosage of SβSS. The formed NCs have
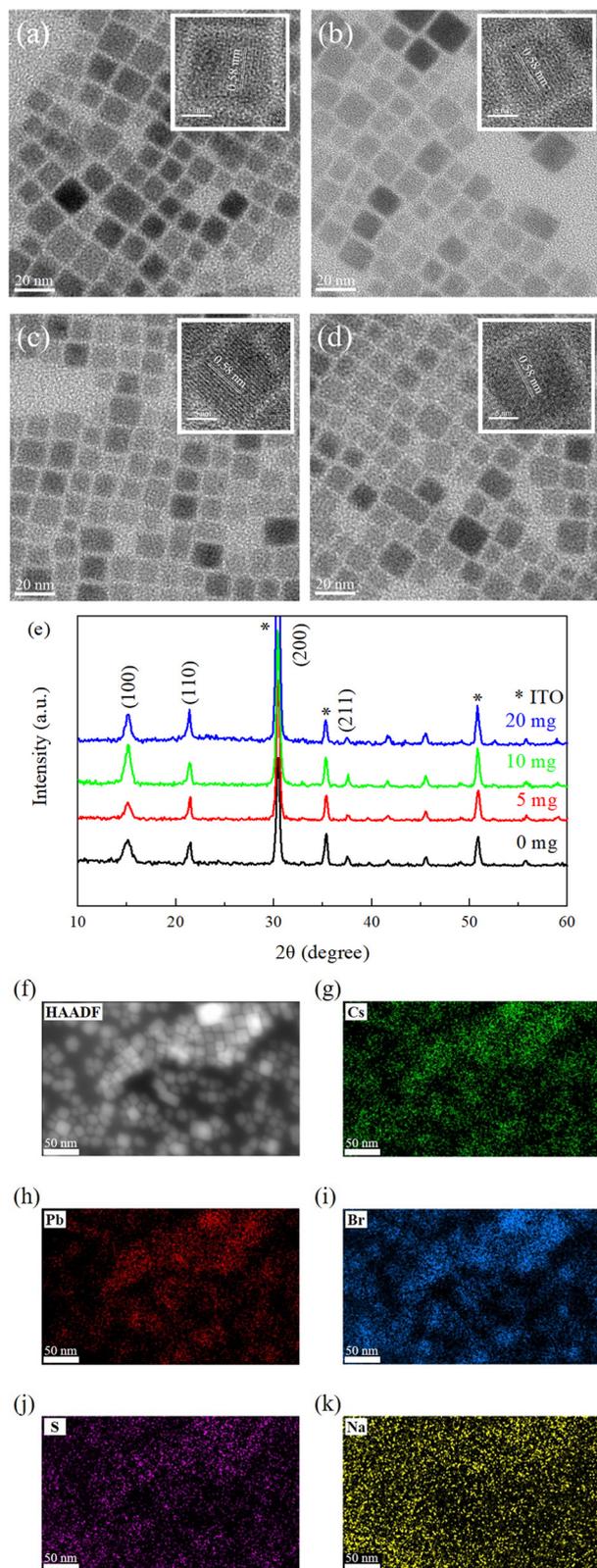
Fig. 2 TEM micrographs of the (a) pristine and SβSS-modified CsPbBr₃ NCs with (b) 5, (c) 10, and (d) 20 mg of SβSS. The insets show the HRTEM images of CsPbBr₃ NCs without and with the SβSS ligand; (e) XRD patterns of the pristine and SβSS-modified CsPbBr₃ NCs; (f) HAADF-STEM and (g–k) elemental mapping of Cs, Pb, Br, S, and Na elements of the SβSS-modified CsPbBr₃ NCs (10 mg).

the highest crystallinity when 10 mg of SβSS is introduced. The crystallinity is then lowered by using 20 mg of SβSS, presumably caused by the overdose. Besides, we notice that the SβSS-modified CsPbBr₃ NCs (10 mg) have the strongest diffraction peak for the (100) plane, indicative of eliminated defects by the passivation process.[46] This observation also implies that the PeLED using the SβSS-modified CsPbBr₃ NCs (10 mg) as the active layer may achieve the best device performance. The high-angle annular dark-field scanning transmission electron microscopy (HAADF-STEM) image and corresponding elemental mapping images of Cs, Pb, Br, S, and Na elements are shown in Fig. 2f and (g–k), respectively. It is clearly seen that the distribution of Cs, Pb, Br, and S elements matches well with the HAADF-STEM image, while Na elements are homogeneously distributed in the detection area. This confirms that the SβSS ligand was anchored on the surface of CsPbBr₃ NCs, and Na ions were randomly dispersed instead of incorporation into the lattice of CsPbBr₃ NCs. To further confirm the existence of the SβSS ligand, FT-IR and ^{1}H NMR experiments were carried out. The FT-IR spectra of SβSS, pristine and SβSS-modified CsPbBr₃ NCs are displayed in Fig. S2 in the ESI.† The absorption bands at 2850–2950 cm^{-1} originated from alkyl chains of OA and OAm ligands for the pristine and SβSS-modified CsPbBr₃ NCs. The characteristic bands in the region of 3015–3092 cm^{-1} are assigned to the =C–H stretching modes of the vinyl protons and benzene ring, which are observed for the SβSS ligand and SβSS-modified CsPbBr₃ NCs. In addition, the ^{1}H NMR spectra of SβSS, pristine and SβSS-modified CsPbBr₃ NCs are shown in Fig. S3 (ESI†). For SβSS, the peaks at around 6.9 ppm are assigned to protons on the vinyl group and multiple signals at around 7.2–7.5 ppm are derived from protons on the benzene ring. These proton signals can also be observed for the SβSS-modified CsPbBr₃ NCs, indicative of the existence of SβSS on the perovskite NCs. Besides, the vinyl protons of OA/OAm are found at 5.3 ppm. The relative proportion of the surface ligands SβSS to OA/OAm is calculated to be 1 : 5 from peak areas of their vinyl protons.

To investigate the existence of SβSS ligands and interaction between CsPbBr₃ and SβSS, XPS measurements on the pristine and SβSS-modified CsPbBr₃ NCs (10 mg) were performed. In Fig. 3a, the Pb 4f$_{5/2}$ and 4f$_{7/2}$ core-level signals of the pristine CsPbBr₃ NCs are observed at 142.6 and 137.7 eV, respectively, which are in accordance with the previous literature.[47,48] Furthermore, the Pb 4f$_{5/2}$ and 4f$_{7/2}$ core-level signals of SβSS-modified CsPbBr₃ NCs (10 mg) shift to higher binding energies at 142.9 and 138.0 eV, respectively, which can be explained by the stronger interaction between SβSS and CsPbBr₃ NCs. Fig. 3b demonstrates the S 2p$_{1/2}$ and 2p$_{3/2}$ core-level signals of SβSS-modified CsPbBr₃ NCs (10 mg) at 169.9 and 168.2 eV, confirming the existence of SβSS ligands on CsPbBr₃ NCs.[49] Fig. S4 (ESI†) displays the Na 1s core-level signals of the pristine and SβSS-modified CsPbBr₃ NCs. It can be clearly observed that the Na 1s core-level signal increases with increasing amounts of SβSS ligands. The low intensity of the Na 1s signal suggests that the Na content in the final CsPbBr₃ NCs was low, i.e., most Na ions were removed after the purification process.

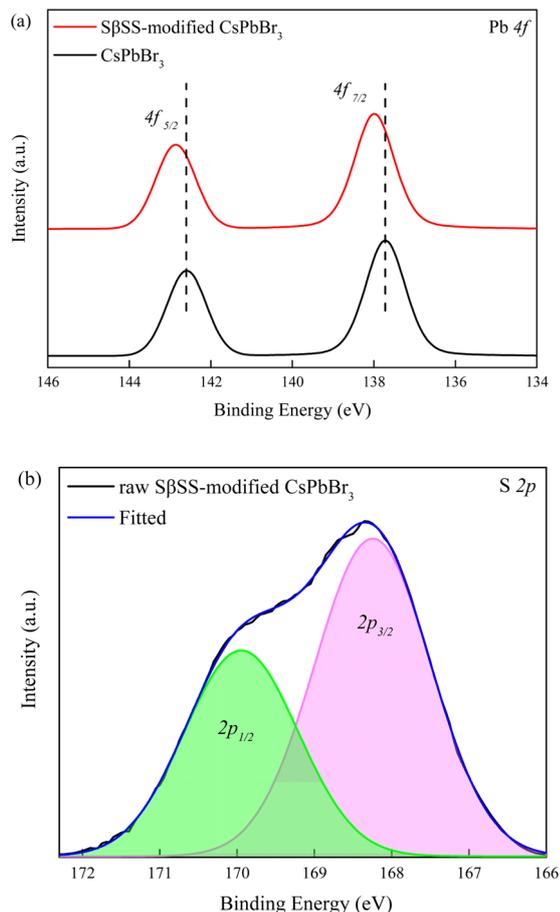The UV-vis absorption spectra of the pristine and SβSS-modified CsPbBr₃ NCs with different SβSS amounts are depicted

Fig. 3 XPS spectra of (a) Pb 4f and (b) S 2p elements in the pristine and SβSS-modified CsPbBr$_3$ NCs (10 mg).

in Fig. 4a–d. The absorption edge of the pristine CsPbBr$_3$ NCs is located at 534 nm, corresponding to an optical E_g of 2.32 eV. After adding SβSS ligands, the absorption edges of the modified CsPbBr$_3$ NCs were gradually blue-shifted to 525, 521, and 520 nm on introducing SβSS amounts of 5, 10, and 20 mg, respectively. The E_g values were slightly increased to be 2.36, 2.38, and 2.39 eV. The PL emission spectra of all samples are also shown in Fig. 4a–d. Similar to UV-vis absorption spectra, the max PL wavelength was also blue-shifted from 515 to 512 nm with increasing SβSS amounts. The blue shift in UV-vis absorption and PL emission is obtained owing to the quantum confinement effect, which is in agreement with reduced crystalline sizes from TEM observation.[34] Besides, the PL maxima of the synthesized CsPbBr$_3$ NCs are located at slightly lower wavelengths than the absorption edge. A similar phenomenon has been reported in the previous literature. Rogach *et al.* synthesized the perovskite CsPb$_x$Cu$_y$(Br/Cl)$_3$ which showed a PL peak at 453 nm and an absorption edge at 465 nm.[50] Chen, Tseng and coworkers reported CsPbBr$_3$ NCs with PL emission and absorption edge at 515 and 525 nm, respectively.[51] All samples exhibit a green emission with a narrow FWHM value of 30 nm. The PLQY as a function of the SβSS amount is displayed in Fig. 4e. Without the introduction of the SβSS ligand, the PLQY of the pristine

CsPbBr$_3$ NCs was estimated to be *ca.* 53%. Noticeably, by adding 10 mg of the SβSS ligand, the PLQY of the modified CsPbBr$_3$ NCs was enhanced to 75%. The reason for the increased PLQY can be ascribed to reduced surface traps to enhance radiative recombination, as shown in Fig. 1c, which has been extensively reported in the literature.[30,33–35,38] By incorporating more of the SβSS ligand up to 20 mg, however, the PLQY was slightly reduced to 72%. Besides, the TR-PL measurement was performed to verify the PLQY trend and PL lifetime of the pristine and SβSS-modified CsPbBr$_3$ NCs. The TR-PL decay curves are shown in Fig. 4f, which are fitted by a biexponential decay model.[52] The average PL lifetimes are calculated to be 3.4, 3.5, 5.0, and 3.8 ns for CsPbBr$_3$ NCs with 0, 5, 10, and 20 mg of the SβSS ligand, respectively. The results from TR-PL measurements are in accordance with the PLQY trend and 10 mg SβSS-modified CsPbBr$_3$ NCs possess the longest lifetime among all samples. On the basis of the PLQY and TR-PL experimental results, introducing an appropriate amount of the SβSS ligand can not only reduce the trap states on the nanocrystalline surface through passivation but also enhance radiative recombination which is beneficial for device performance of PeLEDs. Fig. S5 (ESI†) shows the thermal stability test for the pristine and SβSS-modified CsPbBr$_3$ NCs. The experiment was carried out by continuously heating the two samples at 100 °C. The PL intensities of the pristine and SβSS-modified CsPbBr$_3$ NCs reduced to 50% of their initial values after 60 and 130 min, respectively. We can find out that the stability of the SβSS-modified CsPbBr$_3$ NCs is better than the pristine one.

The PeLED with the ITO/PEDOT:PSS/Poly-TPD/CsPbBr$_3$ NCs/TPBi/LiF/Al structure is demonstrated in Fig. 5a, using the pristine and SβSS-modified CsPbBr$_3$ NCs as the active layers. The energy level diagram of PeLEDs is depicted in Fig. 5b. The energy levels of PEDOT:PSS, poly-TPD, TPBi, and LiF/Al were referred to the previous literature.[53] As for the valence band (VB) and conduction band (CB) of CsPbBr$_3$ NCs, the UPS technique was applied and corresponding UPS spectra are revealed in Fig. S6 in the ESI.† The Fermi level (E_F) was evaluated by subtracting the secondary electron cutoff position from the incident He I photon energy ($h\nu$ = 21.22 eV) to be −3.45 and −3.51 eV for the pristine and SβSS-modified CsPbBr$_3$ NCs, respectively.[54] The VB levels are then deduced to be −5.78 and −5.68 eV from the VB region. By combining with the E_g values, the CB levels can be determined to be −3.46 and −3.3 eV, respectively, for the pristine and SβSS-modified CsPbBr$_3$ NCs. As seen in Fig. 5b, the energy barrier between Poly-TPD and the SβSS-modified CsPbBr$_3$ NCs is smaller as compared with the pristine one, indicating that hole carriers can be transported more efficiently to the SβSS-modified CsPbBr$_3$ NCs to enhance charge recombination. The cross-sectional SEM image of the device is exhibited in Fig. 5c, indicating layer thicknesses of 30, 20, 35, and 100 nm for PEDOT:PSS/Poly-TPD, CsPbBr$_3$ NCs, TPBi, and LiF/Al, respectively. Fig. 5(d–f) present the current density–voltage–brightness, current efficiency–current density characteristics, and EL spectra of PeLEDs based on the pristine and SβSS-modified CsPbBr$_3$ NCs, respectively. It is seen that PeLEDs based on the SβSS-modified CsPbBr$_3$ NCs
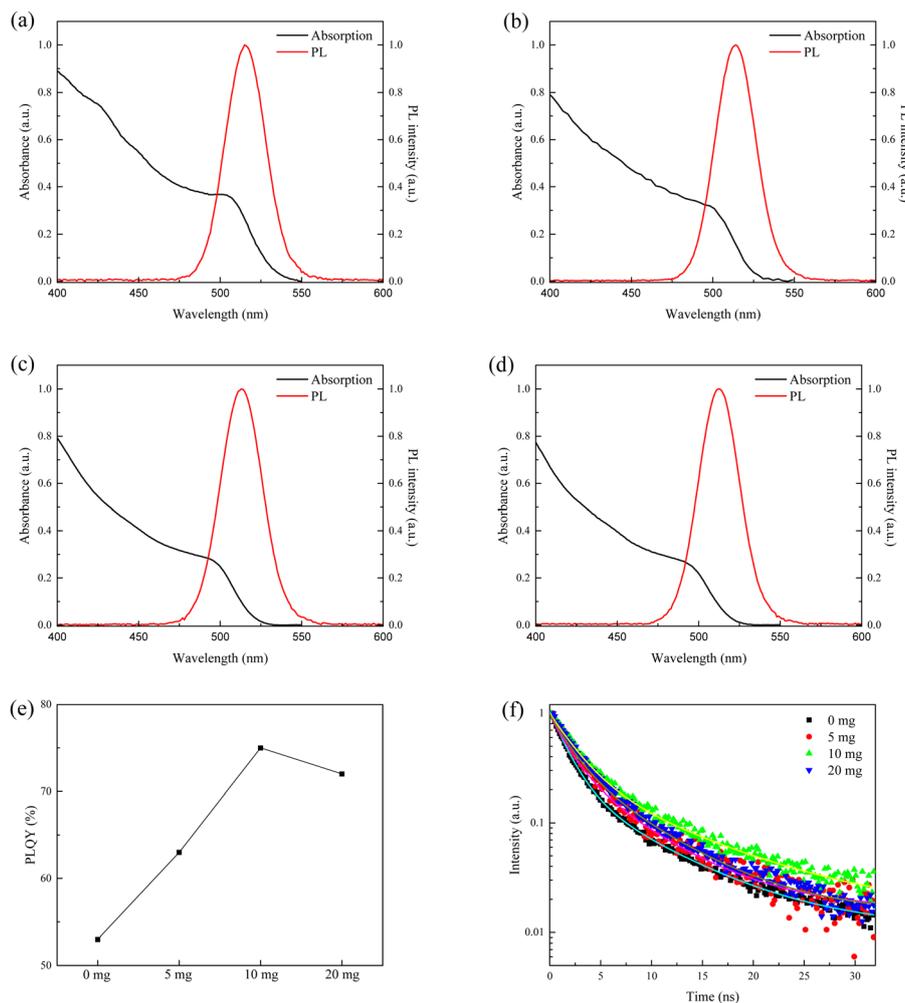
Fig. 4 (a–d) Absorption and PL emission spectra, (e) PLQY as a function of the SβSS amount, and (f) TR-PL decay curves of the pristine and SβSS-modified CsPbBr$_3$ NCs.

exhibited a higher current density than those based on the pristine CsPbBr$_3$ NCs at the same voltage. Furthermore, the threshold voltage of the device was decreased to 3.5 V with increasing amount of SβSS (10 and 20 mg). The augmented current density can be attributed to easier carrier injection caused by surrounding SβSS ligands with π-conjugation, while the pristine CsPbBr$_3$ NCs are capped with long alkylated OAm and OA ligands which hinders charge injection and transport capability.[55] To understand the effect of the SβSS ligand on the carrier injection into CsPbBr$_3$ cores, electron- and hole-only devices were fabricated and corresponding current density–voltage characteristics are shown in Fig. S7 (ESI†). For both electron- and hole-only devices, the current density based on the SβSS-modified CsPbBr$_3$ NCs was higher than that of the pristine one, demonstrating improved electron/hole injection abilities. This is attributed to the elongated π-conjugation of SβSS that helps to improve the carrier injection. The L_{max} and η_{max} of the optimized PeLEDs based on 10 mg SβSS-modified CsPbBr$_3$ NCs were found to be 10 965 cd m^{-2} and 10.9 cd A^{-1}, respectively, revealing about 2.5- and 2.4-fold enhancement compared with the pristine one (L_{max} = 4390 cd m^{-2} and η_{max} = 4.5 cd A^{-1}). In our previous report,

diphenylammonium bromide was utilized as the surface ligand to synthesize CsPbBr$_3$ NCs and the corresponding device performance was moderate (L_{max} = 2011 cd m^{-2} and η_{max} = 2.0 cd A^{-1}).[39] In this study, the SβSS ligand with elongated π-conjugation was adopted and much higher device performance was achieved. By using 5 mg SβSS-modified CsPbBr$_3$ NCs as the active layer, the device revealed a L_{max} of 5018 cd m^{-2} and a η_{max} of 10.1 cd A^{-1}. After the introduction of more of the SβSS ligand up to 20 mg, the device showed a close L_{max} of 10 258 cd m^{-2} and a lower η_{max} of 8.4 cd A^{-1}. The EL spectra of the four PeLEDs at 8 V are shown in Fig. 5f, indicative of green emission at 515–517 nm with a narrow FWHM of about 20 nm. In addition, the EL maxima of PeLEDs are also blue-shifted on increasing the SβSS amount, which is similar to PL observation in Fig. 4b. We confirmed that the FWHM of the EL peak is narrower than that of the PL one. This behavior has also been reported for perovskite nanocrystals in the previous literature. Zeng et al. synthesized blue, green, and red perovskite nanocrystals for fabricating light-emitting diodes.[56] The EL spectra of the blue and green perovskite nanocrystals showed narrower FWHM values (20–23 nm) than PL spectra (FWHM of 23–29 nm). Lee, Kang and coworkers
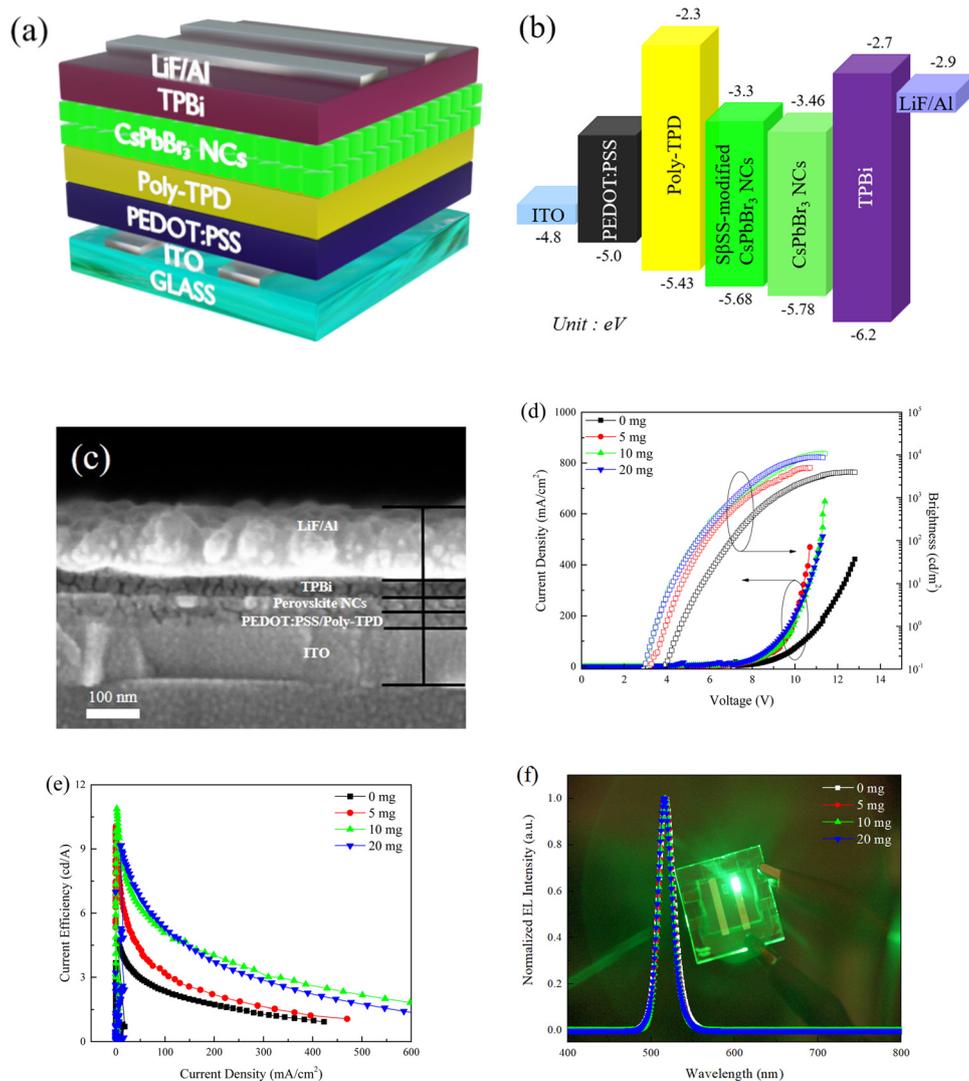
Fig. 5 (a) Device structure, (b) energy level diagram, (c) cross-sectional SEM image, (d) current density–voltage–brightness, (e) current efficiency–current density, and (f) EL spectra of the PeLEDs.

reported PeLEDs based on the CsPbBr$_3$ emitters. The FWHM of the EL spectra was also smaller than that of PL spectra.[37] The corresponding device performance is summarized in Table 1. Besides, no additional emission from poly-TPD or TPBi was detected, revealing that CsPbBr$_3$ NCs were the only emitter in our device. The EL spectra of the device based on the SβSS-modified CsPbBr$_3$ NCs (10 mg) at 6–10 V are shown in Fig. S8

(ESI†), which retained a stable peak wavelength at 516 nm and close spectral line shape with increasing bias voltage.[42,45]

4. Conclusion

In this work, we introduced the SβSS ligand onto the surface of CsPbBr$_3$ NCs by the hot-injection method. The existence of SβSS ligands on CsPbBr$_3$ NCs was confirmed by TEM elemental mapping and XPS experiments. In addition, stronger inter-action between the SβSS ligand and perovskite NCs was obtained due to the sulfonate group. The UV-vis absorption and PL emission behaviors of CsPbBr$_3$ NCs were slightly blue-shifted on incorporating the SβSS ligand. Since the surface defect of CsPbBr$_3$ NCs was effectively passivated by SβSS, a significant PLQY improvement from 53 to 75% was obtained. The best device was achieved by using 10 mg SβSS-modified CsPbBr$_3$ NCs as the emitter, which exhibited a high L_{max} of 10 963 cd m^{-2} and η_{max} of 10.9 cd A^{-1}. It is evident that

Table 1 Device performance of PeLEDs based on the pristine and SβSS-modified CsPbBr$_3$ NCs

SβSS amount (mg)	EL (nm)	FWHM (nm)	$V_{th}{}^{a}$ (V)	L_{max} (cd m^{-2}@V)	η_{max} (cd A^{-1}@V)
0	517	21	4.7	4390@12.7	4.5@8
5	517	20	3.9	5018@10.7	10.1@5.4
10	516	20	3.5	10 965@11.3	10.9@6
20	515	19	3.5	10 258@11.2	8.4@8

^{a} Defined as the operating voltage when the brightness reached 1 cd m^{-2}.

introducing the SβSS ligand as the surface ligand for passivating surface defects provides an efficient route to improving the quality of CsPbBr$_3$ NCs and performance of PeLEDs.

Author contributions

Conceptualization: C.-H. Kuan and S.-H. Yang; methodology: C.-H. Kuan and S.-H. Yang; investigation: C.-H. Kuan; formal analysis: C.-H. Kuan; resources: S.-H. Yang; supervision: S.-H. Yang; validation: S.-H. Yang; writing – original draft: C.-H. Kuan; writing – review and editing: S.-H. Yang. All authors read and approved the final manuscript.

Conflicts of interest

There are no conflicts to declare.

Acknowledgements

References

1 L. Protesescu, S. Yakunin, M. I. Bodnarchuk, F. Krieg, R. Caputo, C. H. Hendon, R. X. Yang, A. Walsh and M. V. Kovalenko, *Nano Lett.*, 2015, **15**, 3692–3696.

2 G. Nedelcu, L. Protesescu, S. Yakunin, M. I. Bodnarchuk, M. J. Grotevent and M. V. Kovalenko, *Nano Lett.*, 2015, **15**, 5635–5640.

3 J.-N. Yang, Y. Song, J.-S. Yao, K.-H. Wang, J.-J. Wang, B.-S. Zhu, M.-M. Yao, S. U. Rahman, Y.-F. Lan, F.-J. Fan and H.-B. Yao, *J. Am. Chem. Soc.*, 2020, **142**, 2956–2967.

4 Y.-H. Kim, C. Wolf, Y.-T. Kim, H. Cho, W. Kwon, S. Do, A. Sadhanala, C. G. Park, S.-W. Rhee, S. H. Im, R. H. Friend and T.-W. Lee, *ACS Nano*, 2017, **11**, 6586–6593.

5 J. Song, J. Li, X. Li, L. Xu, Y. Dong and H. Zeng, *Adv. Mater.*, 2015, **27**, 7162–7167.

6 R. Begum, X. Y. Chin, B. Damodaran, T. J. N. Hooper, S. Mhaisalkar and N. Mathews, *ACS Appl. Nano Mater.*, 2020, **3**, 1766–1774.

7 A. Swarnkar, A. R. Marshall, E. M. Sanehira, B. D. Chernomordik, D. T. Moore, J. A. Christians, T. Chakrabarti and J. M. Luther, *Science*, 2016, **354**, 92–95.

8 K. Chen, W. Jin, Y. Zhang, T. Yang, P. Reiss, Q. Zhong, U. Bach, Q. Li, Y. Wang, H. Zhang, Q. Bao and Y. Liu, *J. Am. Chem. Soc.*, 2020, **142**, 3775–3783.

9 D. Jia, J. Chen, M. Yu, J. Liu, E. M. J. Johansson, A. Hagfeldt and X. Zhang, *Small*, 2020, **16**, 2001772.

10 S. Yakunin, L. Protesescu, F. Krieg, M. I. Bodnarchuk, G. Nedelcu, M. Humer, G. De Luca, M. Fiebig, W. Heiss and M. V. Kovalenko, *Nat. Commun.*, 2015, **6**, 8056.

11 M. L. De Giorgi, F. Krieg, M. V. Kovalenko and M. Anni, *Sci. Rep.*, 2019, **9**, 17964.

12 Q. Chen, J. Wu, X. Ou, B. Huang, J. Almutlaq, A. A. Zhumekenov, X. Guan, S. Han, L. Liang, Z. Yi, J. Li, X. Xie, Y. Wang, Y. Li, D. Fan, D. B. L. Teh, A. H. All, O. F. Mohammed, O. M. Bakr, T. Wu, M. Bettinelli, H. Yang, W. Huang and X. Liu, *Nature*, 2018, **561**, 88–93.

13 P. Ramasamy, D.-H. Lim, B. Kim, S.-H. Lee, M.-S. Lee and J.-S. Lee, *Chem. Commun.*, 2016, **52**, 2067–2070.

14 J. Tao, Z. Xiao, J. Wang, C. Li, X. Sun, F. Li, X. Zou, G. Liao and Z. Zou, *J. Alloys Compd.*, 2020, **845**, 155311.

15 M. Lu, X. Zhang, Y. Zhang, J. Guo, X. Shen, W. W. Yu and A. L. Rogach, *Adv. Mater.*, 2018, **30**, 1804691.

16 M. Liu, N. Jiang, Z. Wang, Y. Zheng, J. Hong, S. Du and D. Chen, *Adv. Photonics Res.*, 2021, **2**, 2100137.

17 S. Thapa, G. C. Adhikari, H. Zhu, A. Grigoriev and P. Zhu, *Sci. Rep.*, 2019, **9**, 18636.

18 Y.-H. Suh, T. Kim, J. W. Choi, C.-L. Lee and J. Park, *ACS Appl. Nano Mater.*, 2018, **1**, 488–496.

19 X. Li, Y. Wu, S. Zhang, B. Cai, Y. Gu, J. Song and H. Zeng, *Adv. Funct. Mater.*, 2016, **26**, 2435–2445.

20 C. K. Ng, W. Yin, H. Li and J. J. Jasieniak, *Nanoscale*, 2020, **12**, 4859–4867.

21 D. Xu, Q. Wan, S. Wu, Y. Zhao, X. Xu, L. Li and G. He, *RSC Adv.*, 2020, **10**, 17653–17659.

22 Y. Cai, Y. Li, L. Wang and R.-J. Xie, *Adv. Opt. Mater.*, 2019, **7**, 1901075.

23 M. Chen, Y. Zou, L. Wu, Q. Pan, D. Yang, H. Hu, Y. Tan, Q. Zhong, Y. Xu, H. Liu, B. Sun and Q. Zhang, *Adv. Funct. Mater.*, 2017, **27**, 1701121.

24 Y. Tong, E. Bladt, M. F. Aygüler, A. Manzi, K. Z. Milowska, V. A. Hintermayr, P. Docampo, S. Bals, A. S. Urban, L. Polavarapu and J. Feldmann, *Angew. Chem., Int. Ed.*, 2016, **55**, 13887–13892.

25 Q. Pan, H. Hu, Y. Zou, M. Chen, L. Wu, D. Yang, X. Yuan, J. Fan, B. Sun and Q. Zhang, *J. Mater. Chem. C*, 2017, **5**, 10947–10954.

26 J. De Roo, M. Ibáñez, P. Geiregat, G. Nedelcu, W. Walravens, J. Maes, J. C. Martins, I. Van Driessche, M. V. Kovalenko and Z. Hens, *ACS Nano*, 2016, **10**, 2071–2081.

27 S. Kumar, J. Jagielski, T. Marcato, S. F. Solari and C.-J. Shih, *J. Phys. Chem. Lett.*, 2019, **10**, 7560–7567.

28 J. Li, L. Xu, T. Wang, J. Song, J. Chen, J. Xue, Y. Dong, B. Cai, Q. Shan, B. Han and H. Zeng, *Adv. Mater.*, 2017, **29**, 1603885.

29 H. Wu, Y. Zhang, M. Lu, X. Zhang, C. Sun, T. Zhang, V. L. Colvin and W. W. Yu, *Nanoscale*, 2018, **10**, 4173–4178.

30 Y. Huang, W. Luan, M. Liu and L. Turyanska, *J. Mater. Chem. C*, 2020, **8**, 2381–2387.

31 J. H. Park, A.-Y. Lee, J. C. Yu, Y. S. Nam, Y. Choi, J. Park and M. H. Song, *ACS Appl. Mater. Interfaces*, 2019, **11**, 8428–8435.

32 Y. Tan, Y. Zou, L. Wu, Q. Huang, D. Yang, M. Chen, M. Ban, C. Wu, T. Wu, S. Bai, T. Song, Q. Zhang and B. Sun, *ACS Appl. Mater. Interfaces*, 2018, **10**, 3784–3792.

33 M. Lu, J. Guo, S. Sun, P. Lu, X. Zhang, Z. Shi, W. W. Yu and Y. Zhang, *Chem. Eng. J.*, 2021, **404**, 126563.

34 J. Zhang, C. Yin, F. Yang, Y. Yao, F. Yuan, H. Chen, R. Wang, S. Bai, G. Tu and L. Hou, *J. Phys. Chem. Lett.*, 2021, **12**, 2437–2443.

35 L. Zhang, Q. Zhang, X. Xing, Y. Jiang, T. He, Y. Huang, Z. Ma, J. Yang and M. Yuan, *ChemNanoMat*, 2019, **5**, 318–322.

36 J. Pan, Y. Shang, J. Yin, M. De Bastiani, W. Peng, I. Dursun, L. Sinatra, A. M. El-Zohry, M. N. Hedhili, A.-H. Emwas, O. F. Mohammed, Z. Ning and O. M. Bakr, *J. Am. Chem. Soc.*, 2018, **140**, 562–565.

37 S. He, N. Kumar, H. Beng Lee, K.-J. Ko, Y.-J. Jung, J. I. Kim, S. Bae, J.-H. Lee and J.-W. Kang, *Chem. Eng. J.*, 2021, **425**, 130678.

38 G. Li, J. Huang, H. Zhu, Y. Li, J.-X. Tang and Y. Jiang, *Chem. Mater.*, 2018, **30**, 6099–6107.

39 R.-H. Shen, S.-H. Yang and P.-Y. Lin, *ACS Appl. Electron. Mater.*, 2020, **2**, 1619–1627.

40 Y. Zu, J. Dai, L. Li, F. Yuan, X. Chen, Z. Feng, K. Li, X. Song, F. Yun, Y. Yu, B. Jiao, H. Dong, X. Hou, M. Ju and Z. Wu, *J. Mater. Chem. A*, 2019, **7**, 26116–26122.

41 J. Dai, J. Xi, Y. Zu, L. Li, J. Xu, Y. Shi, X. Liu, Q. Fan, J. Zhang, S. Wang, F. Yuan, H. Dong, B. Jiao, X. Hou and Z. Wu, *Nano Energy*, 2020, **70**, 104467.

42 J. Pradhan, P. Moitra, Umesh, B. Das, P. Mondal, G. S. Kumar, U. K. Ghorai, S. Acharya and S. Bhattacharya, *Chem. Mater.*, 2020, **32**, 7159–7171.

43 S. Thapa, K. Bhardwaj, S. Basel, S. Pradhan, C. J. Eling, A. M. Adawi, J.-S. G. Bouillard, G. J. Stasiuk, P. Reiss, A. Pariyar and S. Tamang, *Nanoscale Adv.*, 2019, **1**, 3388–3391.

44 Y. Lu, Z. Wang, J. Chen, Y. Peng, X. Tang, Z. Liang, F. Qi and W. Chen, *J. Lumin.*, 2021, **234**, 117952.

45 L. Yang, B. Fu, X. Li, H. Chen and L. Li, *J. Mater. Chem. C*, 2021, **9**, 1983–1991.

46 C. Zheng, C. Bi, F. Huang, D. Binks and J. Tian, *ACS Appl. Mater. Interfaces*, 2019, **11**, 25410–25416.

47 Y. Xie, B. Peng, I. Bravić, Y. Yu, Y. Dong, R. Liang, Q. Ou, B. Monserrat and S. Zhang, *Adv. Sci.*, 2020, **7**, 2001698.

48 M. Liu, G. Zhong, Y. Yin, J. Miao, K. Li, C. Wang, X. Xu, C. Shen and H. Meng, *Adv. Sci.*, 2017, **4**, 1700335.

49 M. Wang, M. Zhou, L. Zhu, Q. Li and C. Jiang, *Sol. Energy*, 2016, **129**, 175–183.

50 C. Bi, S. Wang, Q. Li, S. V. Kershaw, J. Tian and A. L. Rogach, *J. Phys. Chem. Lett.*, 2019, **10**, 943–952.

51 C.-C. Lin, S.-Y. Yeh, W.-L. Huang, Y.-X. Xu, Y.-S. Huang, T.-H. Yeh, C.-H. Tien, L.-C. Chen and Z.-L. Tseng, *Polymers*, 2020, **12**, 2243.

52 R. Chen, Y. Xu, S. Wang, C. Xia, Y. Liu, B. Yu, T. Xuan and H. Li, *J. Alloys Compd.*, 2021, **866**, 158969.

53 P. Liu, W. Chen, W. Wang, B. Xu, D. Wu, J. Hao, W. Cao, F. Fang, Y. Li, Y. Zeng, R. Pan, S. Chen, W. Cao, X. W. Sun and K. Wang, *Chem. Mater.*, 2017, **29**, 5168–5173.

54 Z. Hawash, S. R. Raga, D.-Y. Son, L. K. Ono, N.-G. Park and Y. Qi, *J. Phys. Chem. Lett.*, 2017, **8**, 3947–3953.

55 Y.-H. Kim, G.-H. Lee, Y.-T. Kim, C. Wolf, H. J. Yun, W. Kwon, C. G. Park and T.-W. Lee, *Nano Energy*, 2017, **38**, 51–58.

56 J. Song, J. Li, X. Li, L. Xu, Y. Dong and H. Zeng, *Adv. Mater.*, 2015, **27**, 7162–7167.